

MIT Open Access Articles

Sinc interpolation of nonuniform samples

The MIT Faculty has made this article openly available. **Please share** how this access benefits you. Your story matters.

Citation: Maymon, Shay, and Alan V. Oppenheim. "Sinc Interpolation of Nonuniform Samples." IEEE Transactions on Signal Processing 59.10 (2011): 4745–4758.

As Published: <http://dx.doi.org/10.1109/TSP.2011.2160054>

Publisher: Institute of Electrical and Electronics Engineers (IEEE)

Persistent URL: <http://hdl.handle.net/1721.1/72688>

Version: Author's final manuscript: final author's manuscript post peer review, without publisher's formatting or copy editing

Terms of use: Creative Commons Attribution-Noncommercial-Share Alike 3.0



Sinc Interpolation of Nonuniform Samples

Shay Maymon, *Student Member, IEEE*, Alan V. Oppenheim *Life Fellow, IEEE*

Abstract—It is well known that a bandlimited signal can be uniquely recovered from nonuniformly spaced samples under certain conditions on the nonuniform grid and provided that the average sampling rate meets or exceeds the Nyquist rate. However, reconstruction of the continuous-time signal from nonuniform samples is typically more difficult to implement than from uniform samples. Motivated by the fact that sinc interpolation results in perfect reconstruction for uniform sampling, we develop a class of approximate reconstruction methods from nonuniform samples based on the use of time-invariant lowpass filtering, i.e., sinc interpolation. The methods discussed consist of four cases incorporated in a single framework. The case of sub-Nyquist sampling is also discussed and nonuniform sampling is shown as a possible approach to mitigating the impact of aliasing.

Index Terms—Nonuniform sampling, Approximate reconstruction, Lagrange interpolation, Sinc interpolation, Time jitter, Sub-Nyquist sampling

I. INTRODUCTION

DISCRETE-time signals can arise in many ways, but they most commonly occur as representations of sampled continuous-time signals. The most common form of sampling used in the context of discrete-time processing of continuous-time signals is uniform sampling corresponding to samples of continuous-time signals obtained at equally spaced time intervals. Under certain conditions, specified by the Nyquist-Shannon sampling theorem, the original signal can be reconstructed from this set of equally-spaced samples. The reconstruction is done through sinc interpolation¹ corresponding to the impulse response of a linear time-invariant ideal lowpass filter.

In a variety of contexts, nonuniform sampling naturally arises or is preferable to uniform sampling. For example, some biomedical devices utilize low-power sensors that use self-timed circuits, thus removing the need for power-intensive clock buffers and clock distribution. However, these self-timed circuits tend to introduce nonuniformity in the sampling clock [1]. Nonuniform sampling also often arises in time-interleaved analog-to-digital converters, where a signal is passed through multiple parallel channels, each uniformly sampling the signal at the same rate. The output samples of the channels are then multiplexed to obtain a full discrete-time representation of the signal. For the case in which the clock phases of these channels are asynchronous, interleaving samples from each channel leads to recurrent nonuniform sampling [2]. Recurrent nonuniform sampling also often arises in sensor networks in which each sensor uniformly samples the environment

asynchronously and transmits to a main base station, where the samples are interleaved.

In many cases nonuniform sampling is deliberate and advantageous. In the spatial domain, non-uniformity of the spacing of the array elements in an antenna or acoustic sensor array is often part of the array design as a trade off between the length of the array and the number of elements. In ray traced computer graphics, it has been shown that nonuniform sampling yields aliasing that is less conspicuous to the observer [3].

Exact reconstruction of a bandlimited continuous-time signal from nonuniform samples is based on Lagrange interpolation. For the case of uniform sampling, Lagrange interpolation reduces to sinc interpolation and can be approximated with well designed lowpass filtering. When the sampling grid is not uniform, Lagrange interpolation is more difficult as discussed in section II. In this paper we consider sinc interpolation of nonuniform samples as a way to approximately reconstruct the continuous-time signal. A class of approximate reconstruction methods is proposed in which each method corresponds to a different assumption with respect to the knowledge of the exact sampling times and of the probability distribution of their deviation from a uniform sampling grid.

II. RECONSTRUCTION OF BANDLIMITED SIGNALS FROM NONUNIFORM SAMPLES

A variety of approaches to reconstruction of signals from nonuniform samples have been previously proposed and discussed. In a classic paper on nonuniform sampling of bandlimited signals [2], Yen introduced several reconstruction theorems to address the cases of a finite number of nonuniform samples on an otherwise uniform grid, a single gap in uniform sampling and recurrent nonuniform sampling. Other reconstruction approaches, specific to recurrent nonuniform sampling have also been proposed [4–8]. In the work of Yao and Thomas [9], the Lagrange interpolation functions were applied to the reconstruction of bandlimited signals from nonuniform samples. It is shown there that a finite-energy signal $x(t)$ bandlimited to $\pm\pi/T_N$ can be reconstructed from its nonuniform samples $x(t_n)$ using Lagrange interpolation when the sampling instants t_n do not deviate by more than $T_N/4$ from a uniform grid with spacing of T_N . Specifically, if

$$|t_n - nT_N| \leq d < T_N/4, \quad \forall n \in \mathbb{Z}, \quad (1)$$

then

$$x(t) = \sum_{n=-\infty}^{\infty} x(t_n) l_n(t), \quad (2a)$$

where

$$l_n(t) = \frac{G(t)}{G'(t_n)(t - t_n)}, \quad (2b)$$

This work was supported in part by a Fulbright Fellowship, Texas Instruments Leadership University Program, and BAE Systems PO 112991.

¹Throughout the paper we refer to convolution of an impulse train of samples with the function $h(t) = \text{sinc}(\frac{\pi}{T}t)$ as sinc interpolation and use the historical unnormalized definition of the sinc function, i.e. $\text{sinc}(x) \triangleq \frac{\sin(x)}{x}$.

$$G(t) = (t - t_0) \prod_{\substack{k=-\infty \\ k \neq 0}}^{\infty} \left(1 - \frac{t}{t_k}\right), \quad (2c)$$

and $G'(t) \triangleq \frac{dG(t)}{dt}$. Interpolation using eqs. (2) is referred to as Lagrange interpolation. This theorem is based on a theorem proved by Levinson [10], which states that the functions $\{L_n(\Omega)\}$, defined as the Fourier transforms of $\{l_n(t)\}$, are bandlimited and form a sequence biorthogonal to $\{e^{j\Omega t_n}\}$ over $[-\frac{\pi}{T_N}, \frac{\pi}{T_N}]$, given that the condition of eq. (1) is satisfied, i.e.,

$$L_n(\Omega) = \int_{-\infty}^{\infty} l_n(t) e^{-j\Omega t} dt = 0, \quad |\Omega| > \frac{\pi}{T_N}, \quad (3)$$

and

$$\frac{1}{2\pi} \int_{-\frac{\pi}{T_N}}^{\frac{\pi}{T_N}} L_n(\Omega) e^{j\Omega t_k} d\Omega = l_n(t_k) = \delta[n - k]. \quad (4)$$

Eq. (4) utilizes the interpolation condition of the Lagrange kernel which ensures that the property of consistent resampling is upheld, i.e., that sampling the reconstructed signal on the nonuniform grid $\{t_n\}$ yields the original samples $\{x(t_n)\}$. Note that expressing $L_n(\Omega)$ in (4) as the Fourier transform of $l_n(t)$ results in biorthogonality of the sequences $\{l_n(t)\}$ and $\{\text{sinc}(\pi/T_N(t - t_n))\}$, i.e.,

$$\int_{-\infty}^{\infty} l_n(t) \text{sinc}(\pi/T_N(t - t_k))/T_N dt = \delta[n - k], \quad (5)$$

from which the expansion in (2) for bandlimited signals is clearly followed.

The difficulty of exact reconstruction of bandlimited signals from nonuniform samples through Lagrange interpolation is partly due to the fact that the interpolating functions at different sampling times do not have the same form except in special cases. Also, each interpolating function depends on all sampling instants. The complexity of the implementation motivates the need for simpler approximate approaches to reconstruction, and a variety of methods has previously been proposed. One practical approach to recovering a signal from its nonuniform samples has been the use of nonuniform splines [11]. Iterative reconstruction methods for nonuniform sampling which are computationally demanding and have potential issues of convergence have also been previously proposed [12–18]. In a different approach, time-warping methods were applied by Papoulis in [19] to reconstruct bandlimited signals from jittered samples. In [20] and [21], time-warping was used for reconstruction from samples of signals with time-varying frequency content. A method of designing FIR filters in such a way that the effect of input clock jitter is diminished is discussed in [22]. In [23, 24] several approaches are suggested and analyzed for approximate reconstruction from jittered samples. Mean-square comparison of various interpolators is done in [25] for the case of uniform sampling, uniform sampling with skips, and Poisson sampling. A modification of the conventional Lagrange interpolator is proposed in [26] which allows approximating a bandlimited signal from its nonuniform samples with high accuracy. A comprehensive review of literature concerning other techniques in nonuniform sampling can be found in [27] and [28].

III. SINC INTERPOLATION OF NONUNIFORM SAMPLES

In this section we restrict $l_n(t)$ in eq. (2a) to be of the form $l_n(t) = (T/T_N) \text{sinc}(\pi/T_N \cdot (t - \tilde{t}_n))$ corresponding to sinc interpolation. It will be assumed throughout this section that the average sampling rate meets or exceeds the Nyquist rate, i.e., that $T \leq T_N$ where T denotes the nominal sampling interval and T_N denotes the Nyquist sampling interval.

Note that since the kernel used in this framework is time-invariant, the exact sampling instants are not needed in designing the reconstruction filter. This is in contrast to Lagrange interpolation in which this knowledge is required in forming the interpolating functions since these functions do not have the same form at each sampling instant and each interpolating function depends on all sampling instants, i.e., it is not a time-invariant convolution.

We consider and analyze four cases incorporated in a single framework where the choice for the values \tilde{t}_n differs for each of the methods discussed below. In the first case, it is assumed that both the exact sampling instants and the probability distribution of their deviation from a uniform sampling grid are known. As we will see in section III-F, even with the knowledge of the exact sampling instants, it can sometimes be beneficial to place the samples on a grid other than the actual nonuniform grid corresponding to the sampling instants. In determining this grid we utilize the probability distribution of the deviation of the sampling instants from a uniform sampling grid. In the second case, sinc interpolation is applied to the samples placed on a uniform grid with spacing corresponding to the average or nominal spacing of the nonuniform sampling grid. In that approximation it is not necessary to know the exact sampling instants since they are not used. This may occur in situations where the samples are stored in memory and their exact timing information is lost. The third case consists of applying sinc interpolation to the samples located at the actual nonuniform sampling times. This method requires knowledge of the nonuniform grid. However, as opposed to Lagrange interpolation where the sampling instants are needed in advance to generate the interpolating functions, the sinc interpolation function requires only knowledge of the nominal sample spacing. In the fourth case, it is assumed that the exact sampling times are not known but that the probability distribution of their deviation from a uniform sampling grid is known.

A. Mathematical Formulation

To have a common framework that incorporates these four cases, we denote by $x[n]$ a sequence of nonuniform samples of $x(t)$, i.e.,

$$x[n] = x(t_n) \quad (6)$$

where $\{t_n\}$ represent a nonuniform grid which we model as a perturbation of a uniform grid with spacing T , i.e.,

$$t_n = nT + \xi_n. \quad (7)$$

For analysis purposes, we consider $x(t)$ to be a continuous-time zero-mean wide-sense stationary random process with autocorrelation function $R_{xx}(\tau)$ and power spectral density

(PSD) $S_{xx}(\Omega)$ which is zero for $|\Omega| \geq \Omega_c = \pi/T_N$. ξ_n is characterized as an i.i.d. sequence of zero-mean random variables independent of $x(t)$ with probability density function (pdf) $f_\xi(\xi)$ and characteristic function $\Phi_\xi(\Omega) = \int_{-\infty}^{\infty} f_\xi(\xi') e^{j\Omega\xi'} d\xi'$.

For the reconstruction of $x(t)$ from its nonuniform samples $x[n]$, we apply sinc interpolation to the samples placed on a second nonuniform grid $\tilde{t}_n = nT + \zeta_n$ that in general is not restricted to the nonuniform grid on which the samples were originally acquired, i.e., ζ_n and ξ_n are not necessarily equal. The reconstruction takes the form

$$\hat{x}(t) = \sum_{n=-\infty}^{\infty} (T/T_N) \cdot x(t_n) \cdot h(t - \tilde{t}_n), \quad (8)$$

with $h(t) = \text{sinc}(\frac{\pi}{T_N}t)$ as illustrated in Figure 1, where $\frac{\pi}{T_N}$ is the highest frequency present in $x(t)$.

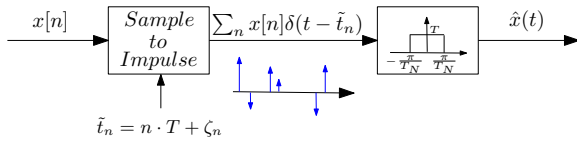


Fig. 1. Reconstruction using sinc interpolation.

The four cases outlined above are incorporated into this general framework as follows: For the first case, we characterize ζ_n as another i.i.d. sequence of random variables independent of $x(t)$ and for which ζ_n is independent of ξ_k when $n \neq k$. This case will be referred to as Randomized Sinc Interpolation (RSI) and is the most general case we consider, since the other three cases can be treated as special cases of it. In the second case, we assume that only the average spacing of the nonuniform grid is known rather than the exact location of the sampling times. This corresponds to choosing $\zeta_n = 0$ and applying sinc interpolation to the samples placed on a uniform grid. We refer to this case as Uniform Sinc Interpolation (USI). The third case referred to as Nonuniform Sinc Interpolation (NSI) corresponds to choosing $\zeta_n = \xi_n$, i.e., the reconstruction is carried out on the nonuniform grid corresponding to the sampling instants. In the fourth case, we assume that the deviations ξ_n of the sampling instants from a uniform grid are not known but their probability distribution is known. Therefore, ζ_n is characterized as an i.i.d. sequence of random variables independent of $x(t)$ and for which ζ_n is independent of ξ_k for all n, k . This case will be referred to as Independent Sinc Interpolation (ISI). Table I summarizes these four cases.

B. Randomized Sinc Interpolation

Appendix B shows an equivalence with respect to second-order statistics² between the nonuniform sampling discussed above when followed by Randomized Sinc Interpolation and the system in Figure 2. The frequency response of the LTI system in Figure 2 is the joint characteristic function $\Phi_{\xi\zeta}(\Omega_1, \Omega_2)$

²Throughout the paper we use the terminology of equivalence between two systems with respect to second-order statistics to mean that for the same input, the output means, auto-correlation functions, and cross-correlation functions are identical.

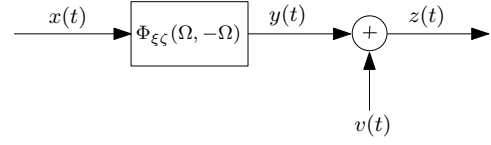


Fig. 2. A second-order statistics model for nonuniform sampling followed by Randomized Sinc Interpolation for the case where $T \leq T_N$.

of ξ_n and ζ_n , defined as the Fourier transform of their joint pdf $f_{\xi\zeta}(\xi, \zeta)$. In the same figure, $v(t)$ is zero-mean additive colored noise, uncorrelated with $x(t)$, with PSD as follows:

$$S_{vv}(\Omega) = \frac{T}{2\pi} \int_{-\Omega_c}^{\Omega_c} S_{xx}(\Omega') (1 - |\Phi_{\xi\zeta}(\Omega', -\Omega)|^2) d\Omega' \quad |\Omega| < \Omega_c.$$

Thus, with respect to second-order statistics, $\hat{x}(t)$ can equivalently be represented by the signal $z(t)$ in Figure 2.

We denote $e^R(t) = \hat{x}(t) - x(t)$ as the error between $x(t)$ and its approximation $\hat{x}(t)$ obtained by RSI. Then, as shown in Appendix B, the corresponding mean square error (MSE) is given by

$$\sigma_{e^R}^2 = \frac{1}{2\pi} \int_{-\Omega_c}^{\Omega_c} S_{xx}(\Omega) \cdot Q(\Omega) d\Omega, \quad (9)$$

where

$$Q(\Omega) = |1 - \Phi_{\xi\zeta}(\Omega, -\Omega)|^2 + \frac{1}{r} \cdot \int_{-\Omega_c}^{\Omega_c} \frac{1 - |\Phi_{\xi\zeta}(\Omega, -\Omega_1)|^2}{2\Omega_c} d\Omega_1, \quad (10)$$

and $r = T_N/T \geq 1$ denotes the oversampling ratio.

C. Uniform Sinc Interpolation

In the case where neither the sampling instants nor their distribution is known, we set the perturbations ζ_n in the reconstruction of Figure 1 to zero. This results in

$$\hat{x}(t) = \sum_{n=-\infty}^{\infty} (T/T_N) \cdot x(t_n) \cdot h(t - nT), \quad (11)$$

which corresponds to treating the nonuniform samples as being on a uniform grid and reconstructing $x(t)$ with sinc interpolation of these samples as though the sampling was uniform, corresponding to USI. Note that when USI is used for reconstruction, the signal $x(t)$ in the equivalent system of Figure 2 is in effect pre-filtered by the characteristic function $\Phi_\xi(\Omega)$ of ξ_n , and the additive uncorrelated noise $v(t)$ is white. Since $|\Phi_\xi(\Omega)| \leq \Phi_\xi(\Omega)|_{\Omega=0} = 1$, the characteristic function has in general the behavior of a lowpass filter when viewed as a frequency response of an LTI system³.

The error between $x(t)$ and its approximation $\hat{x}(t)$ obtained by USI is denoted by $e^U(t)$ and the corresponding MSE follows directly from (9) by replacing $\Phi_{\xi\zeta}(\Omega_1, \Omega_2)$ with

³Note that when ξ_n is symmetrically distributed on $(-T/2, T/2)$, the characteristic function $\Phi_\xi(\Omega)$ is real and symmetric. In addition, in the region $\Omega \in (-\pi/T, \pi/T)$ $\Phi_\xi(\Omega)$ is non-negative, concave and bounded from below by $\cos(\Omega T/2)$, as elaborated in Appendix A. Its radius of curvature at $\Omega = 0$ is also shown to be inversely proportional to the variance σ_ξ^2 of ξ_n .

TABLE I
SINC INTERPOLATION RECONSTRUCTION METHODS

Randomized Sinc Interpolation (RSI) Sinc interpolation is applied to the samples placed on a grid determined by both the exact sampling instants and the pdf of their deviation from a uniform sampling grid	Nonuniform Sinc Interpolation (NSI) Sinc interpolation is applied to the samples placed on the nonuniform grid corresponding to the sampling instants
Independent Sinc Interpolation (ISI) Sinc interpolation is applied to the samples located on a grid independent of the actual nonuniform grid	Uniform Sinc Interpolation (USI) Sinc interpolation is applied to the samples placed on a uniform grid

$\Phi_\xi(\Omega_1)$, i.e.,

$$\sigma_{eU}^2 = \frac{1}{2\pi} \int_{-\Omega_c}^{\Omega_c} S_{xx}(\Omega) \left(|1 - \Phi_\xi(\Omega)|^2 + \frac{1}{r} \cdot \left(1 - |\Phi_\xi(\Omega)|^2 \right) \right) d\Omega. \quad (12)$$

For the case of no oversampling, i.e., when the oversampling factor $r = 1$, the MSE in eq. (12) reduces to

$$\begin{aligned} \sigma_{eU}^2 &= 2 \cdot \frac{1}{2\pi} \int_{-\Omega_c}^{\Omega_c} S_{xx}(\Omega) \cdot (1 - \Re(\Phi_\xi(\Omega))) d\Omega \\ &= 2 \cdot \left(R_{xx}(0) - \frac{1}{2\pi} \int_{-\Omega_c}^{\Omega_c} S_{xx}(\Omega) \cdot \Re(\Phi_\xi(\Omega)) d\Omega \right) \\ &= 2 \cdot \left(R_{xx}(0) - \int_{-\infty}^{\infty} R_{xx}(\tau) \cdot f_\xi^{(\text{even})}(\tau) d\tau \right). \end{aligned} \quad (13)$$

When in addition, ξ_n is symmetrically distributed on $(-T_N/2, T_N/2)$, the following inequalities on the mean square reconstruction error follow by utilizing the properties of $R_{xx}(\tau)$ and $\Phi_\xi(\Omega)$ given in Appendix A,

$$\frac{\sigma_{eU}^2}{2R_{xx}(0)} \geq 1 - \min(\rho_{xx}(\xi_0), \Phi_\xi(\Omega_0)) \quad (14a)$$

$$\frac{\sigma_{eU}^2}{2R_{xx}(0)} \leq 1 - \max(\rho_{xx}(T_N/2), \Phi_\xi(\pi/T_N)), \quad (14b)$$

where $\rho_{xx}(\tau) = R_{xx}(\tau)/R_{xx}(0)$, $\xi_0 = E(|\xi|)$, and $\Omega_0 = \int_{-\Omega_c}^{\Omega_c} |\Omega| \cdot \frac{S_{xx}(\Omega)}{\int_{-\Omega_c}^{\Omega_c} S_{xx}(\Omega') d\Omega'} d\Omega$. The fact that $R_{xx}(\tau)$ is monotonically decreasing in $(0, T_N/2)$ and $\Phi_\xi(\Omega)$ is monotonically decreasing in $(0, \pi/T_N)$ leads to

$$\int_{-T_N/2}^{T_N/2} R_{xx}(\tau) f_\xi(\tau) d\tau \geq R_{xx}(T_N/2), \quad (15)$$

and

$$\frac{1}{2\pi} \int_{-\Omega_c}^{\Omega_c} S_{xx}(\Omega) \cdot \Phi_\xi(\Omega) d\Omega \geq R_{xx}(0) \cdot \Phi_\xi(\pi/T_N), \quad (16)$$

from which the upper bound in (14) clearly follows. To obtain the lower bound in (14) we use the concavity of $R_{xx}(\tau)$ and

$\Phi_\xi(\Omega)$ in the appropriate regions. Specifically,

$$\begin{aligned} \int_{-T_N/2}^{T_N/2} R_{xx}(\tau) f_\xi(\tau) d\tau &= \int_0^{T_N/2} R_{xx}(\tau) \cdot 2f_\xi(\tau) d\tau \\ &\leq R_{xx} \left(\int_0^{T_N/2} \tau \cdot 2f_\xi(\tau) d\tau \right) = R_{xx}(E(|\xi|)), \end{aligned} \quad (17)$$

and

$$\begin{aligned} \frac{1}{2\pi} \int_{-\Omega_c}^{\Omega_c} S_{xx}(\Omega) \cdot \Phi_\xi(\Omega) d\Omega &= \\ R_{xx}(0) \cdot \frac{1}{2\pi} \int_{-\Omega_c}^{\Omega_c} \frac{S_{xx}(\Omega)}{\frac{1}{2\pi} \int_{-\Omega_c}^{\Omega_c} S_{xx}(\Omega') d\Omega'} \cdot \Phi_\xi(\Omega) d\Omega \\ &\leq R_{xx}(0) \cdot \Phi_\xi \left(\int_{-\Omega_c}^{\Omega_c} |\Omega| \cdot \frac{S_{xx}(\Omega)}{\int_{-\Omega_c}^{\Omega_c} S_{xx}(\Omega') d\Omega'} d\Omega \right). \end{aligned} \quad (18)$$

Note that the inequality in (17) suggests that when $E(|\xi|) = \xi_0 < T_N/2$ is fixed, minimum mean square reconstruction error of USI is achieved when ξ_n takes the values $\pm\xi_0$ with equal probabilities, i.e., when $\Phi_\xi(\Omega) = \cos(\xi_0\Omega)$. Alternatively, when $\int_{-\Omega_c}^{\Omega_c} |\Omega| \cdot \frac{S_{xx}(\Omega)}{\int_{-\Omega_c}^{\Omega_c} S_{xx}(\Omega') d\Omega'} d\Omega = \Omega_0 < \pi/T_N$ is fixed, it follows from (18) that minimum mean square reconstruction error of USI is achieved when $\rho_{xx}(\tau) = \cos(\Omega_0\tau)$. The lower bound in (14) together with the fact that when a lower bound is achieved it is the greatest lower bound results in the following upper bounds on $\rho_{xx}(\tau)$ and $\Phi_\xi(\Omega)$,

$$\rho_{xx}(\tau) \leq \cos(\Omega_0\tau) \quad |\tau| < T_N/2, \quad (19)$$

$$\Phi_\xi(\Omega) \leq \cos(\xi_0\Omega) \quad |\Omega| < \pi/T_N. \quad (20)$$

We would expect the performance of USI to be inversely proportional to the signal's bandwidth B_x , as defined in (30). This is intuitively reasonable since with slow variations of the signal, the uniform samples $x(nT_N)$ are accurately approximated by the nonuniform samples $x(t_n)$. The upper bound on σ_{eU}^2 seems to agree with this intuition since it decreases as $R_{xx}(T_N/2)$ increases, and $R_{xx}(T_N/2)$ is expected to increase as the radius of curvature of $R_{xx}(\tau)$ at $\tau = 0$ increases or equivalently as the bandwidth B_x of $x(t)$ decreases.

D. Nonuniform Sinc Interpolation

When the sampling instants t_n are known, we can alternatively set the reconstruction perturbations ζ_n to be equal to the sampling perturbations ξ_n so that the impulses in Figure 1 are located on the correct grid. This is another special case of eq. (8) for which the reconstruction takes the form

$$\hat{x}(t) = \sum_{n=-\infty}^{\infty} (T/T_N) \cdot x(t_n) \cdot h(t - t_n). \quad (21)$$

Note that for this approximation, referred to as Nonuniform Sinc Interpolation, the distribution of the perturbations is not needed. The corresponding MSE of the reconstruction error $e^N(t)$ follows directly from eq. (9) by replacing $\Phi_{\xi\zeta}(\Omega_1, \Omega_2)$ with $\Phi_{\xi}(\Omega_1 - \Omega_2)$, i.e.,

$$\sigma_{e^N}^2 = \frac{1}{r} \cdot \left(R_{xx}(0) - \frac{1}{2\Omega_c} \int_{-\Omega_c}^{\Omega_c} (S_{xx}(\Omega) * |\Phi_{\xi}(\Omega)|^2) d\Omega \right) = \frac{1}{r} \cdot \frac{1}{2\pi} \int_{-\Omega_c}^{\Omega_c} S_{xx}(\Omega) \cdot \left(\int_{\Omega - \Omega_c}^{\Omega + \Omega_c} \frac{1 - |\Phi_{\xi}(\Omega')|^2}{2\Omega_c} d\Omega' \right) d\Omega. \quad (22)$$

E. Independent Sinc Interpolation

When the exact sampling times are not known but the probability distribution $f_{\xi}(\xi)$ of their deviation from a uniform sampling grid is known, and choosing ζ_n in the reconstruction of Figure 1 to be independent of ξ_k for all n, k , we obtain

$$\sigma_{e^I}^2 = \frac{1}{2\pi} \int_{-\Omega_c}^{\Omega_c} S_{xx}(\Omega) \cdot \left\{ |1 - \Phi_{\xi}(\Omega) \Phi_{\zeta}(-\Omega)|^2 + \frac{1}{r} \cdot \left(1 - |\Phi_{\xi}(\Omega)|^2 \cdot \frac{1}{2\Omega_c} \int_{-\Omega_c}^{\Omega_c} |\Phi_{\zeta}(\Omega_1)|^2 d\Omega_1 \right) \right\} d\Omega. \quad (23)$$

As with any characteristic function, $|\Phi_{\zeta}(\Omega)| \leq 1$ for all Ω . Consequently, the second term in eq. (23) is minimized when $\Phi_{\zeta}(\Omega) = 1$, corresponding to $\zeta_n = 0$, i.e., Uniform Sinc Interpolation. In minimizing the first term in eq. (23) we restrict $f_{\xi}(\xi)$ to be symmetric. Furthermore, the deviation from the uniform grid is restricted to be less than $T/2$, i.e., $f_{\xi}(\xi) = 0$ for $|\xi| \geq T/2$. From this it follows that the Fourier transform of $f_{\xi}(\xi)$, i.e., $\Phi_{\xi}(\Omega)$ is guaranteed to be real and non-negative for $|\Omega| \leq \pi/T$ (see Appendix A). Since the average sampling rate is at or above the Nyquist rate, i.e., $\frac{\pi}{T} \geq \Omega_c$, $\Phi_{\xi}(\Omega)$ will always be real and non-negative in the interval of integration for the first term in eq. (23). Consequently, to minimize that term we again choose $\Phi_{\zeta}(\Omega) = 1$, corresponding to Uniform Sinc Interpolation.

In summary, when the probability density function of ξ_n is symmetric and has bounded support, Uniform Sinc Interpolation is an optimal reconstruction within this framework. More generally, the optimal choice for $f_{\zeta}(\zeta)$ may not correspond to Uniform Sinc Interpolation and lower MSE may be achieved with $\Phi_{\zeta}(\Omega) = e^{-j\zeta_0\Omega}$ corresponding to $\zeta_n = -\zeta_0$, i.e., Uniform Sinc Interpolation with an offset of the uniform grid. The offset ζ_0 can be optimized to minimize $\sigma_{e^I}^2$ in (23). Specifically,

$$\zeta_0^{opt} = \arg \max_{\zeta_0} \Re \left\{ \frac{1}{2\pi} \int_{-\Omega_c}^{\Omega_c} S_{xx}(\Omega) \Phi_{\xi}(\Omega) e^{j\zeta_0\Omega} d\Omega \right\} \quad (24)$$

or equivalently,

$$\begin{aligned} \zeta_0^{opt} &= \arg \max_{\zeta_0} R_{xx}(\tau) * f_{\xi}(\tau)|_{\tau=\zeta_0} \\ &= \arg \max_{\zeta_0} E_{\xi} (R_{xx}(\xi - \zeta_0)). \end{aligned} \quad (25)$$

Note that when $f_{\xi}(\xi)$ is symmetric and the deviation from the uniform grid is less than $T/2$, $\zeta_0^{opt} = 0$ consistent with the observation that the optimal reconstruction in this case does not depend on the specific shape of the pdf and corresponds to Uniform Sinc Interpolation. This follows by noting that

$$\begin{aligned} &\int_{-T/2}^{T/2} R_{xx}(\tau - \zeta_0) f_{\xi}(\tau) d\tau = \\ &\int_0^{T/2} [R_{xx}(\tau - \zeta_0) + R_{xx}(\tau + \zeta_0)] f_{\xi}(\tau) d\tau \leq \\ &\int_{-T/2}^{T/2} R_{xx}(\tau) f_{\xi}(\tau) d\tau, \end{aligned} \quad (26)$$

where we used the symmetry of the pdf $f_{\xi}(\xi)$ and of $R_{xx}(\tau)$, and the property that

$$R_{xx}(\tau) \geq \frac{1}{2} (R_{xx}(\tau - \zeta_0) + R_{xx}(\tau + \zeta_0)) \quad \forall |\tau| < T/2, \zeta_0, \quad (27)$$

which Appendix A shows to be true for the autocorrelation function of a bandlimited signal.

F. RSI - Minimum Mean Square Reconstruction Error

As eq. (9) shows, the performance of RSI depends on the power spectrum $S_{xx}(\Omega)$ of the continuous-time signal $x(t)$ as well as on the joint characteristic function $\Phi_{\xi\zeta}(\Omega_1, \Omega_2)$ of the perturbations, which can be designed to reduce the MSE. In order to formulate the optimal reconstruction within the framework of RSI, i.e., to design ζ_n in the reconstruction method of Figure 1 to achieve minimum MSE, eq. (9) should be optimized with respect to $\Phi_{\xi\zeta}(\Omega_1, \Omega_2)$ subject to the constraint $\Phi_{\xi\zeta}(\Omega, 0) = \Phi_{\xi}(\Omega)$. This optimization requires in general the knowledge of both the exact sampling instants and the probability distribution of their deviation from a uniform sampling grid. As we will next see, even though the exact sampling instants are known, the optimal reconstruction may not correspond to NSI, i.e., the optimal grid on which the samples are placed in reconstruction prior to sinc interpolation may possibly be different than the actual nonuniform sampling grid.

In minimizing the MSE we consider two cases. The first is the case of small, zero-mean perturbations from a uniform grid, for which in the region $|\Omega_1| < \Omega_c$ and $|\Omega_2| < \Omega_c$, $\Phi_{\xi\zeta}(\Omega_1, \Omega_2)$ can be approximated well by the second-order Taylor expansion

$$\Phi_{\xi\zeta}(\Omega_1, \Omega_2) \approx 1 - \sigma_{\xi\zeta}\Omega_1\Omega_2 - \frac{1}{2}\sigma_{\xi}^2\Omega_1^2 - \frac{1}{2}\sigma_{\zeta}^2\Omega_2^2, \quad (28)$$

with the corresponding standard deviations σ_{ξ} and σ_{ζ} of ξ_n and ζ_n assumed to be small enough relative to T so that (28)

holds. Substituting (28) into (9) for the case $r = 1$ yields

$$\sigma_{e_R}^2 \approx R_{xx}(0) \cdot (\sigma_\xi^2 \cdot B_x + 1/3 \cdot \sigma_\zeta^2 \cdot \Omega_c^2), \quad (29)$$

where B_x is a measure of the signal's bandwidth defined as

$$B_x = \int_{-\Omega_c}^{\Omega_c} \Omega^2 \cdot \left(\frac{S_{xx}(\Omega)}{\int_{-\Omega_c}^{\Omega_c} S_{xx}(\Omega') d\Omega'} \right) d\Omega. \quad (30)$$

From (29) we see that independent of the detailed characteristics of the perturbation or the signal spectrum, as long as the perturbations around the uniform grid are small enough so that (28) holds, it is preferable to reconstruct the signal using USI, corresponding to $\zeta_n = 0$. This is despite the fact that USI uses only the nominal rather than actual sampling times.

We next consider the case in which the sampling perturbation errors are uniformly distributed over the range $(-\frac{T}{2}, \frac{T}{2})$. As previously mentioned, the optimal perturbations ζ_n in the reconstruction of Figure 1 are chosen to minimize (9) with respect to $\Phi_{\xi\zeta}(\Omega_1, \Omega_2)$. One interesting case occurs when the joint characteristic function $\Phi_{\xi\zeta}(\Omega_1, \Omega_2)$ is characterized by a finite set of parameters, and the optimization of the MSE in (9) reduces to optimization over those parameters. Consider as an example the case when ζ_n is a k^{th} -order polynomial of ξ_n whose coefficients are to be designed. For simplicity, we consider here only the linear case, i.e., $\zeta_n = \beta \xi_n$ with $\beta \in [0, 1]$ for which the case of $\beta = 0$ corresponds to USI and the case of $\beta = 1$ corresponds to NSI. It then follows that the Fourier transform of the joint pdf $f_{\xi\zeta}(\xi, \zeta)$ is

$$\Phi_{\xi\zeta}(\Omega_1, \Omega_2) = \Phi_\xi(\Omega_1 + \beta\Omega_2), \quad (31)$$

and $Q(\Omega)$ as defined in (10) reduces to

$$Q(\Omega) = |1 - \Phi_\xi((1 - \beta)\Omega)|^2 + \frac{1}{r} \cdot \int_{-\Omega_c}^{\Omega_c} \frac{|1 - \Phi_\xi(\Omega - \beta\Omega_1)|^2}{2\Omega_c} d\Omega_1, \quad (32)$$

where $\Phi_\xi(\Omega) = \text{sinc}(\frac{T}{2}\Omega)$. Figure 3 shows $Q(\Omega)$ for different values of β with no oversampling, i.e., when the oversampling factor $r = 1$. As indicated, at low frequencies $Q(\Omega)$ is minimized when β is close to 0, whereas at high frequencies it is minimized when β is close to 1. More generally, the optimal choice of β that minimizes the reconstruction MSE will depend on the specific shape of the power spectrum $S_{xx}(\Omega)$ of the input signal $x(t)$. As Figure 3 suggests, it will tend to be small for signals that vary slowly, i.e., when B_x as defined in (30) is small. As an illustration, Figure 4 demonstrates this behavior of the optimal choice of β as a function of B_x for an example in which $S_{xx}(\Omega)$ is of the form

$$S_{xx}(\Omega) = \frac{\pi}{d \tan(\Omega_c/d)} \cdot \frac{1}{1 + (\Omega/d)^2} \quad |\Omega| < \Omega_c, \quad (33)$$

in which case

$$B_x = \frac{\Omega_c d}{\arctan(\Omega_c/d)} - d^2, \quad (34)$$

and

$$\frac{1}{2\pi} \int_{-\Omega_c}^{\Omega_c} S_{xx}(\Omega) d\Omega = 1. \quad (35)$$

As indicated, when the bandwidth B_x of the input signal is small, the samples are positioned close to the uniform sampling grid. As B_x is increased, β is increased and as a result the samples are positioned closer to their original locations but still with a tendency towards the uniform grid due to the optimality of USI.

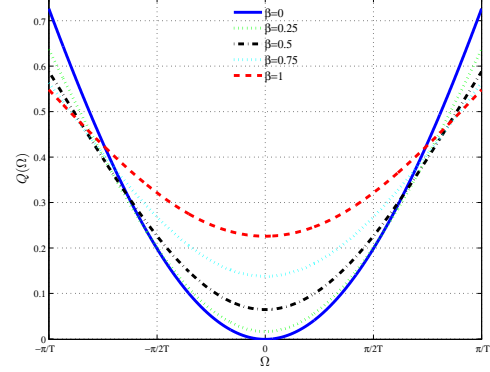


Fig. 3. $Q(\Omega)$ for the case where $\xi_n \sim u[-T/2, T/2]$ and $T = T_N = 1$.

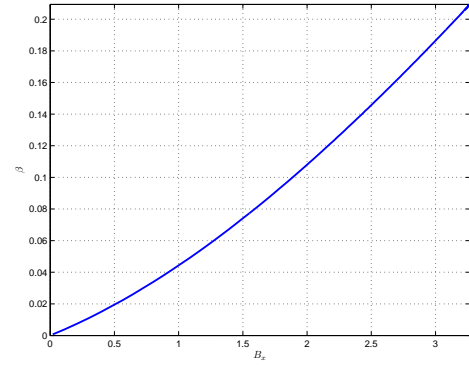


Fig. 4. The optimal choice of β that minimizes $\sigma_{e_R}^2$ as a function of B_x for the case where $T = T_N = 1$.

G. Discussion

While USI uses only the zero-mean assumption of the perturbation error and does not require the knowledge of the exact sampling instants, this knowledge is necessary for NSI. Comparing USI with NSI with respect to mean square reconstruction error, it is in general not possible to claim which of these methods is preferable. Their relative performance is dependent on the power spectrum $S_{xx}(\Omega)$ of the continuous-time signal, the distribution $f_\xi(\xi)$ of the sampling perturbations and the oversampling ratio r . For ISI, not only the mean but the entire probability distribution function of the deviation from a uniform sampling grid is needed in general. Since USI can be viewed as a special case of ISI for which $f_\zeta(\zeta) = \delta(\zeta)$, it might be possible in general to obtain a lower MSE with ISI than with USI. As previously discussed, there are cases in which even though the entire probability distribution of the sampling perturbations is known, the mean square reconstruction error of ISI is minimized when $f_\zeta(\zeta) = \delta(\zeta)$, corresponding to USI. USI, NSI and ISI can all

be formulated as special cases of RSI, which is more general. With an appropriate choice of $f_{\xi\zeta}(\xi, \zeta)$, it might be possible in general to obtain a lower MSE with RSI than with USI, NSI or ISI.

In the problem formulation, the samples were taken on a nonuniform grid that is a perturbation of a uniform grid, and the objective was to design the grid on which to locate the samples in reconstruction prior to sinc interpolation. Nevertheless, this framework can handle other cases of interest as well. Consider for example the case in which the samples are taken on an accurate uniform grid, but there are timing inaccuracies in the discrete to continuous processing. This case can be formed as a special case of the general framework for which $\Phi_{\xi\zeta}(\Omega_1, \Omega_2) = \Phi_{\zeta}(\Omega_2)$.

IV. SUB-NYQUIST SAMPLING

In the previous section we considered the case of $T \leq T_N$ for which under certain conditions perfect reconstruction is possible using Lagrange interpolation. When $T > T_N$ perfect reconstruction is in general not possible. However, the biorthogonality condition in (4) guarantees that whether or not $T \leq T_N$, the output of the system in Figure 5 with $l_n(t)$ as given by eq. (2b) corresponds to the least-squares approximation of $x(t)$. In other words, when the sampling

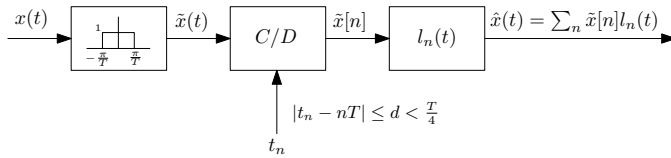


Fig. 5. Anti-Aliasing followed by nonuniform sampling and Lagrange interpolation.

instants $\{t_n\}$ satisfy the condition

$$|t_n - nT| \leq d < T/4 \quad \forall n \in \mathbb{Z}, \quad (36)$$

the use of an anti-aliasing LTI filter with cut-off frequency of half the average sampling rate, followed by nonuniform sampling and Lagrange interpolation results in an orthogonal projection from the space of finite energy signals to the subspace of finite energy bandlimited signals.

In certain applications, it is either not possible or not preferable to implement anti-aliasing filtering. With uniform sampling and when the Nyquist condition is not satisfied, frequency components of the original signal that are higher than half the sampling rate are then folded into lower frequencies resulting in aliasing. More generally, when the sampling grid is nonuniform and satisfies the condition of eq. (36), the approximation resulting from Lagrange interpolation can be viewed in general as an oblique projection from the space of finite energy signals into the space of finite energy bandlimited signals. This follows from noting that the composition of sampling at times $\{t_n\}$ and reconstruction using the kernel $l_n(t)$ is a linear operator $f(\cdot)$. Since the Lagrange kernel is bandlimited, applying the operator $f(\cdot)$ to $x(t)$ yields a bandlimited signal $\hat{x}(t) = f(x(t))$. Since Lagrange interpolation results in perfect reconstruction from nonuniform samples

of bandlimited signals, $f(\hat{x}(t)) = f(x(t))$, i.e., $f(\cdot)$ is a projection. Consequently, aliasing with uniform or nonuniform sampling is a projection from the space of out of band signals into the space of bandlimited signals [29]. The projection representing aliasing with nonuniform sampling is in general an oblique rather than orthogonal projection.

Nonuniform sampling can offer an advantage over uniform sampling when the nominal sampling rate is less than the Nyquist rate, i.e., for undersampled signals. It has previously been suggested by several authors that nonuniform sampling can be utilized to mitigate the impact of aliasing. In certain applications, particularly perceptual ones, the distortion resulting from nonuniform sampling is often preferable to aliasing artifacts. In fact, a form of randomized sampling is used in the computer graphics community to anti-alias ray-traced images [3, 30, 31]. In this section we consider the framework developed in section III for reconstruction from nonuniform samples for the case where $T > T_N$, i.e., sub-Nyquist sampling and discuss the second-order statistics characteristics and the aliasing behavior of these methods.

A. Randomized Sinc Interpolation

Applying Randomized Sinc Interpolation to the nonuniform samples $\{x(t_n)\}$ as shown in Figure 1, where the cut-off frequency of the ideal low-pass filter is $\frac{\pi}{T}$, results in $\hat{x}(t)$ whose power spectrum and cross-correlation with $x(t)$ are shown in Appendix C to be

$$S_{\hat{x}\hat{x}}(\Omega) = \sum_{n=-\infty}^{\infty} S_{xx}(\Omega - \frac{2\pi}{T}n) |\Phi_{\xi\zeta}(\Omega - \frac{2\pi}{T}n, -\Omega)|^2 + \frac{T}{2\pi} \int_{-\Omega_c}^{\Omega_c} S_{xx}(\Omega') \left(1 - |\Phi_{\xi\zeta}(\Omega', -\Omega)|^2\right) d\Omega' \quad |\Omega| < \frac{\pi}{T}, \quad (37)$$

and

$$R_{\hat{x}x}(t, t - \tau) = \frac{1}{2\pi} \int_{-\pi/T}^{\pi/T} e^{j\Omega\tau} \cdot \sum_{n=-\infty}^{\infty} \left(S_{xx} \left(\Omega - \frac{2\pi}{T}n \right) \cdot \Phi_{\xi\zeta} \left(\Omega - \frac{2\pi}{T}n, -\Omega \right) e^{j\frac{2\pi}{T}n(t-\tau)} \right) d\Omega = \int_{-\infty}^{\infty} R_{xx}(t_1) \cdot \sum_{n=-\infty}^{\infty} \left[f_{\xi\zeta}(t_1 + t - nT - \tau, \zeta) * \text{sinc}\left(\frac{\pi}{T}\zeta\right) \right] |_{\zeta=t-nT} dt_1. \quad (38)$$

Once again, the perturbations in sampling and reconstruction can be designed to shape the power spectrum of the reconstructed signal through the joint characteristic function $\Phi_{\xi\zeta}(\Omega_1, \Omega_2)$. Notice that in the case of $T = T_N$, eqs. (37) and (38) coincide with the output power spectrum and the input-output cross-correlation of the system in Figure 2.

B. Uniform Sinc Interpolation

In the case of Uniform Sinc Interpolation, sinc interpolation is applied to the samples placed on a uniform grid with spacing corresponding to the average spacing of the nonuniform sampling grid. With respect to second-order statistics, nonuniform sampling followed by USI is equivalent to the system of Figure 6, in which $v^U(t)$ is zero-mean additive white noise,

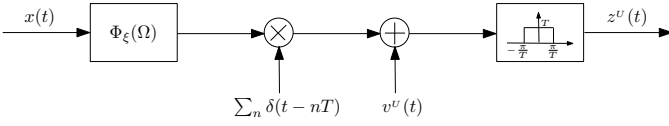


Fig. 6. A second-order statistics equivalent of nonuniform sampling followed by Uniform Sinc Interpolation for the case where $T > T_N$.

uncorrelated with $x(t)$. For the system of Figure 6 it is straight forward to show that

$$S_{z^U z^U}(\Omega) = \sum_{n=-\infty}^{\infty} S_{xx} \left(\Omega - \frac{2\pi}{T}n \right) \cdot \left| \Phi_{\xi} \left(\Omega - \frac{2\pi}{T}n \right) \right|^2 + \underbrace{\frac{T}{2\pi} \int_{-\Omega_c}^{\Omega_c} S_{xx}(\Omega') \cdot \left(1 - |\Phi_{\xi}(\Omega')|^2 \right) d\Omega'}_{T^2 \cdot S_{v^U v^U}(\Omega)} \quad |\Omega| < \frac{\pi}{T}, \quad (39)$$

and that

$$R_{z^U x}(t, t - \tau) = \frac{1}{2\pi} \int_{-\pi/T}^{\pi/T} \sum_{n=-\infty}^{\infty} \left(S_{xx} \left(\Omega - \frac{2\pi}{T}n \right) \cdot \Phi_{\xi} \left(\Omega - \frac{2\pi}{T}n \right) e^{j\frac{2\pi}{T}n(t-\tau)} \right) e^{j\Omega\tau} d\Omega. \quad (40)$$

To show the equivalence, we note that with Uniform Sinc Interpolation, i.e., when $\zeta_n = 0$, $S_{\hat{x}\hat{x}}(\Omega)$ in eq. (37) reduces to $S_{z^U z^U}(\Omega)$ in eq. (39) and the cross-correlation $R_{\hat{x}x}(t, t - \tau)$ in eq. (38) reduces to $R_{z^U x}(t, t - \tau)$ in eq. (40). The structure of Figure 6 suggests that with respect to second-order statistics, nonuniform sampling with stochastic perturbations can be modeled as uniform sampling of the signal pre-filtered by the Fourier transform of the pdf of the sampling perturbation. Correspondingly, the pdf $f_{\xi}(\xi)$ can be designed subject to the constraints on $f_{\xi}(\xi)$ as a probability density function so that the characteristic function $\Phi_{\xi}(\Omega)$ acts as an equivalent anti-aliasing LPF. Of course the stochastic perturbation still manifests itself through the additive white noise source $v^U(t)$ in Figure 6. Thus, Figure 6 suggests that aliasing can be traded off with uncorrelated white noise by appropriate design of the pdf of the sampling perturbation.

C. Nonuniform Sinc Interpolation

In the case of Nonuniform Sinc Interpolation, sinc interpolation is applied to the samples located at the actual nonuniform sampling grid. With respect to second-order statistics this is equivalent to the system in Figure 7, in which $v^N(t)$ is zero-

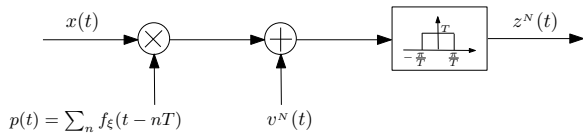


Fig. 7. A second-order statistics equivalent of nonuniform sampling followed by Nonuniform Sinc Interpolation for the case where $T > T_N$.

mean additive noise, uncorrelated with $x(t)$. For the system

of Figure 7 it is straight forward to show that

$$S_{z^N z^N}(\Omega) = \sum_{n=-\infty}^{\infty} S_{xx} \left(\Omega - \frac{2\pi}{T}n \right) \cdot \left| \Phi_{\xi} \left(\frac{2\pi}{T}n \right) \right|^2 + \underbrace{\frac{T}{2\pi} \int_{-\Omega_c}^{\Omega_c} S_{xx}(\Omega') \cdot \left(1 - |\Phi_{\xi}(\Omega - \Omega')|^2 \right) d\Omega'}_{T^2 \cdot S_{v^N v^N}(\Omega)} \quad |\Omega| < \frac{\pi}{T}, \quad (41)$$

and that

$$R_{z^N x}(t, t - \tau) = \int_{-\infty}^{\infty} R_{xx}(\tau - \tau') p(t - \tau') \text{sinc} \left(\frac{\pi}{T} \tau' \right) d\tau', \quad (42)$$

where $p(t) = \sum_{n=-\infty}^{\infty} f_{\xi}(t - nT)$. The equivalence is shown by noting that with Nonuniform Sinc Interpolation, i.e., when $\zeta_n = \xi_n$, $S_{\hat{x}\hat{x}}(\Omega)$ in eq. (37) reduces to $S_{z^N z^N}(\Omega)$ in eq. (41) and $R_{\hat{x}x}(t, t - \tau)$ in eq. (38) reduces to $R_{z^N x}(t, t - \tau)$ in eq. (42).

Figure 7 suggests that with respect to second-order statistics, nonuniform sampling followed by NSI is equivalent to modulating the signal with a periodic signal $p(t)$ with period T , obtained from the pdf $f_{\xi}(\xi)$ of the perturbation error and adding uncorrelated noise. In the frequency domain, this corresponds to scaling each replica of the spectrum by $|\Phi_{\xi}(\frac{2\pi}{T}n)|^2$. Correspondingly, the components in (41) associated with aliasing can be eliminated by designing the pdf $f_{\xi}(\xi)$ so that $\Phi_{\xi}(\frac{2\pi}{T}n) = 0$ for all $n \neq 0$, which corresponds in the time-domain to $p(t) = c$ where c is a nonzero constant. Of course, similar to USI, the stochastic perturbation still manifests itself through additive uncorrelated noise, as shown in Figure 7. However, as opposed to USI where the additive noise is white and the signal is pre-filtered by the characteristic function of the perturbation, the additive noise in NSI is in general not white, its power spectrum is determined by the convolution of $S_{xx}(\Omega)$ with $(1 - |\Phi_{\xi}(\Omega)|^2)$, and the shape of the original signal is preserved in reconstruction.

D. Independent Sinc Interpolation

With respect to second-order statistics, Independent Sinc Interpolation corresponds to the system of Figure 8, in which

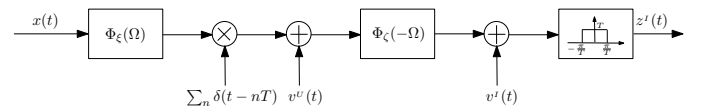


Fig. 8. A second-order statistics equivalent of nonuniform sampling followed by Independent Sinc Interpolation for the case where $T > T_N$.

$v^I(t)$ is zero-mean additive noise, uncorrelated with both $v^U(t)$ and $x(t)$,

$$R_{z^I x}(t, t - \tau) = \frac{1}{2\pi} \int_{-\pi/T}^{\pi/T} \sum_{n=-\infty}^{\infty} \left(S_{xx} \left(\Omega - \frac{2\pi}{T}n \right) \cdot \Phi_{\xi} \left(\Omega - \frac{2\pi}{T}n \right) e^{j\frac{2\pi}{T}n(t-\tau)} \right) \Phi_{\xi}(-\Omega) e^{j\Omega\tau} d\Omega, \quad (43)$$

and

$$S_{z^I z^I}(\Omega) = \left(\sum_{n=-\infty}^{\infty} S_{xx} \left(\Omega - \frac{2\pi}{T}n \right) \left| \Phi_{\xi} \left(\Omega - \frac{2\pi}{T}n \right) \right|^2 + \underbrace{\frac{T}{2\pi} \int_{-\Omega_c}^{\Omega_c} S_{xx}(\Omega') \left(1 - |\Phi_{\xi}(\Omega')|^2 \right) d\Omega'}_{T^2 \cdot S_{v_v U}(\Omega)} \right) \cdot |\Phi_{\xi}(-\Omega)|^2 + \underbrace{(1 - |\Phi_{\xi}(-\Omega)|^2) \cdot \frac{T}{2\pi} \int_{-\Omega_c}^{\Omega_c} S_{xx}(\Omega') d\Omega'}_{T^2 \cdot S_{v_v I}(\Omega)} \quad |\Omega| < \frac{\pi}{T}. \quad (44)$$

As Figure 8 suggests, perturbing the grid on which the samples are placed prior to sinc interpolation has a similar effect to that of the stochastic perturbations in sampling, i.e., the characteristic function of the perturbations acts as a low-pass filter and an uncorrelated noise is added.

E. Simulations

In Figure 10 we illustrate the different types of artifacts resulting from sub-Nyquist sampling and with each of the reconstruction methods discussed above. We choose the signal $x(t)$ to be the output of an LTI system driven by white noise for which the transfer function $H_c(s)$ has unity gain at $s = 0$, and as shown in Figure 9 its poles and zeros locations are $\{0.1\pi e^{j\pi(2k+9)/20}\}_{k=1}^{10}$ and $\{0.1\pi(-0.1 \pm \frac{5}{8}j)\}$, respectively.

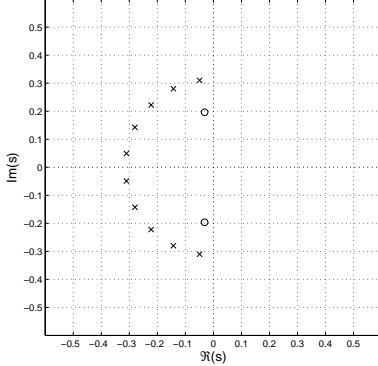


Fig. 9. Pole-zero diagram of the transfer function $H_c(s)$.

To simulate a discrete-time signal whose power spectrum is consistent with the power spectrum of $x(t)$, we process discrete-time white noise with a discrete-time LTI system whose impulse response $h[n]$ is obtained using the method of impulse invariance, i.e., by sampling the impulse response $h_c(t)$ of the continuous-time system every $T_d = 1$ [sec]. The spacing on this grid is considered to be sufficiently dense so that aliasing is negligible and it accurately represents the impulse response of the continuous-time system. Figure 10(a) shows $\hat{S}_{xx}(\Omega)$, the estimated power spectrum of $x(t)$ obtained by applying Welch's method [32] with Hanning window of length 6656 [sec] and with 50% overlap. 500 blocks are averaged to obtain the estimate. This method and parameters are used for all spectral estimates in Figure 10.

From the parameters used for generating $x(t)$ and consistent with Figure 10(a) we consider the bandwidth of $x(t)$ to be approximately 0.14 π [rad/sec] and the corresponding value of T_N to be approximately 7 [sec]. In the remaining simulations in Figure 10, the average or nominal spacing is $T = 13$ [sec] $\approx 1.8T_N$, and the power spectrum estimates are shown over the region $[-\frac{\pi}{T}, \frac{\pi}{T}]$ as if an ideal reconstruction filter was applied.

Figure 10(b) corresponds to the case of uniform sampling where reconstruction is obtained by applying USI to the samples of $x(t)$. This figure shows the estimated PSD $\hat{S}_{xx}^U(\Omega)$ of the approximation obtained by simulations vs. the theoretical results of the PSD and its components as follows from eq. (39) for the uniform sampling case, i.e., when $\xi_n = 0$. As shown in this figure, aliasing occurs as a result of undersampling and the interference is therefore correlated with the signal. (c), (d) and (e) of Figure 10 correspond to reconstruction obtained by applying USI, NSI and ISI respectively to the nonuniform samples of $x(t)$ with $T = 13$ [sec], and the deviation ξ_n from a uniform sampling grid uniformly distributed over $(-T/2, T/2)$. Those figures compare the estimated PSD $\hat{S}_{xx}^{USI}(\Omega)$, $\hat{S}_{xx}^{NSI}(\Omega)$ and $\hat{S}_{xx}^{ISI}(\Omega)$ obtained by simulations with the theoretical results, as in eqs. (39), (41) and (44), respectively. As shown in (b)-(e) of Figure 10, the theoretical results are consistent with those obtained by simulations.

Consistent with the fact that the characteristic function $\Phi_{\xi}(\Omega)$ of the sampling perturbations acts as an anti-aliasing filter in the model of Figure 6, the aliasing produced in USI as shown in Figure 10(c) is reduced relative to that produced with uniform sampling. However, this reduced aliasing is at the expense of an additional additive uncorrelated white noise component. Note that in Figure 10(d) there is no aliasing but only uncorrelated noise. This is because the pdf $f_{\xi}(\xi)$ of the perturbations satisfies the following condition

$$\Phi_{\xi} \left(\frac{2\pi}{T}n \right) = 0 \quad \forall n \neq 0, \quad (45)$$

which ensures no aliasing artifact when applying NSI to the nonuniform samples. Figure (e) corresponds to ISI with ζ_n uniformly distributed over $(-T/2, T/2)$. Comparing this figure with figure (c), we notice that due to the filtering by the characteristic function $\Phi_{\xi}(-\Omega)$ of the perturbations ζ_n as shown in Figure 8, high frequency components of the signal and its replicas are attenuated in ISI compared to USI, and the additive uncorrelated noise is appropriately shaped. Superimposed on $\hat{S}_{xx}(\Omega)$ are shown in Figure 10(f) the estimated PSD of the various approximations obtained by simulations of the reconstruction methods discussed above.

As we can see from these figures, the artifacts resulting in sub-Nyquist sampling differ in each of the reconstruction methods discussed above and can be controlled by designing the perturbations in sampling and in reconstruction to trade off aliasing with uncorrelated noise. The artifacts correspond to uniform sampling are more severe in high frequencies and are correlated with the signal, whereas the artifacts correspond to the reconstruction methods from nonuniform sampling have reduced or no correlation with the signal and are more balanced across frequency.

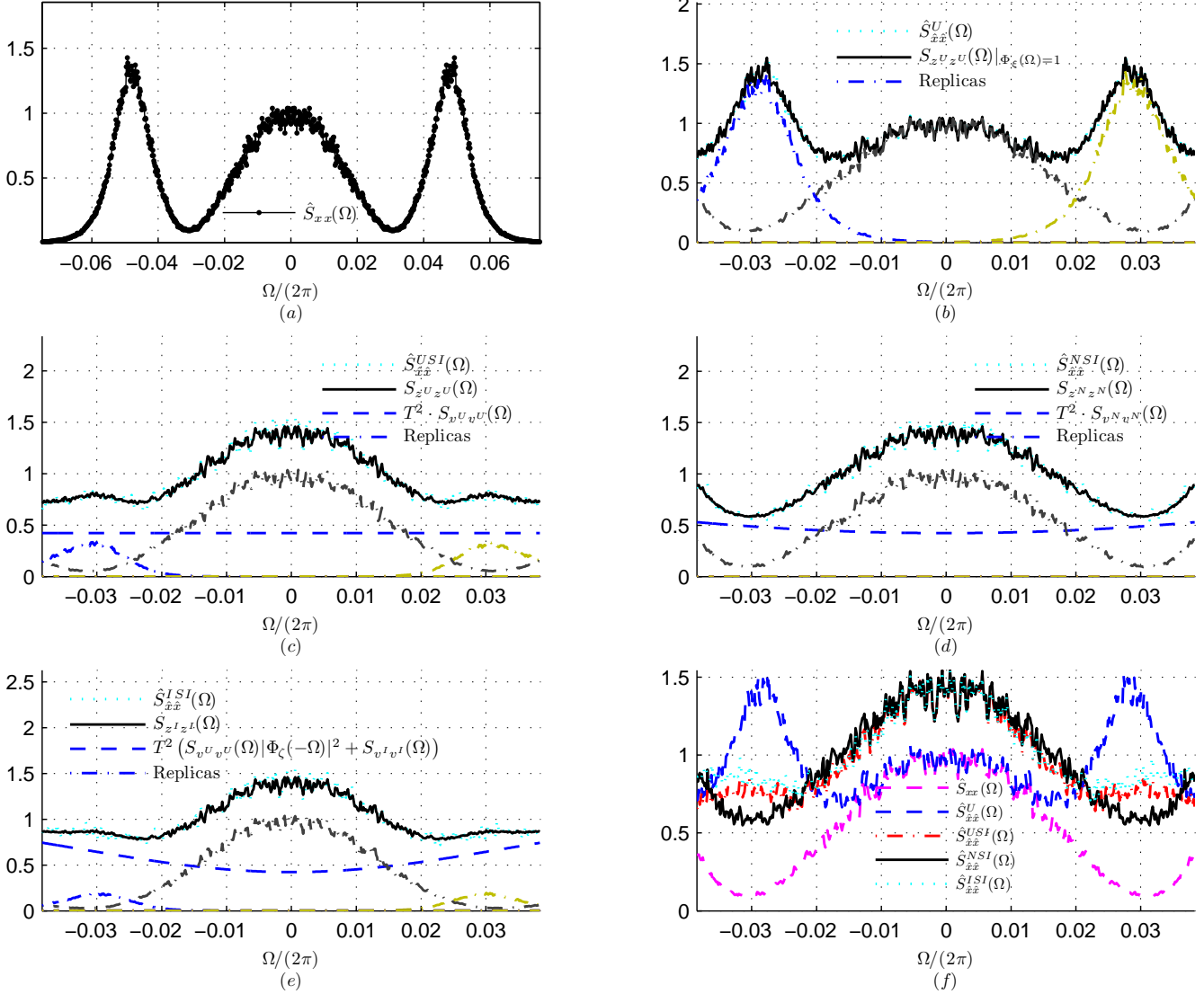


Fig. 10. Artifacts with sub-Nyquist sampling. (a) The estimated power spectrum of $x(t)$. The estimated power spectrum vs. analytic results in the case of (b) Uniform Sampling, (c) USI applied to nonuniform sampling, (d) NSI applied to nonuniform sampling, and (e) ISI applied to nonuniform sampling. (f) The estimated power spectrum of $x(t)$ and of its approximations.

V. CONCLUSIONS

A class of approximate reconstruction methods from non-uniform samples based on sinc interpolation is developed in which each method corresponds to a different assumption with respect to the knowledge of the exact sampling times and of the probability distribution of their deviation from a uniform sampling grid. The methods discussed consist of four cases incorporated in a single framework. The performance of the reconstruction methods is analyzed and compared with respect to the reconstruction MSE. When the perturbations around the uniform grid are small, USI is preferable within this framework even though it uses the least amount of information. When the exact sampling times are not known but the probability distribution of their deviation from a uniform grid is known and symmetric and has bounded support, USI is optimal independent of the shape of the pdf of the perturbations. More generally, optimal reconstruction may not

correspond to USI and better performance may be achieved with Uniform Sinc Interpolation with an offset of the uniform grid determined by the autocorrelation function of the input signal and the pdf of the sampling perturbations. The case of sub-Nyquist sampling is also discussed and analysis based on second-order statistics is derived. With respect to second-order statistics, each of the methods discussed is shown to be equivalent to a simple system consisting of modulation with a periodic signal. The artifacts due to undersampling differ in each of the methods and can be controlled by designing the perturbations in sampling and in reconstruction to trade off aliasing with uncorrelated noise.

APPENDIX A

THE FOURIER TRANSFORM OF A NON-NEGATIVE REAL SYMMETRIC FUNCTION WHOSE SUPPORT IS BOUNDED

The following properties are generally true for any function whose Fourier transform pair is non-negative real, symmetric, and has bounded support (e.g. the characteristic function of a symmetric pdf whose support is bounded). For convenience and without loss of generality, we express these properties in terms of the autocorrelation function of a bandlimited signal. We denote by $R_{xx}(\tau)$ the autocorrelation function of a bandlimited signal $x(t)$ whose power spectrum $S_{xx}(\Omega) = 0$ for all $\Omega \geq \pi/T_N$. Then, the following properties hold:

1) Non-negativity -

$$R_{xx}(\tau) > 0 \quad \forall |\tau| < T_N/2,$$

2) For all ζ_0

$$R_{xx}(\tau) \geq \frac{1}{2} (R_{xx}(\tau - \zeta_0) + R_{xx}(\tau + \zeta_0)) \quad \forall |\tau| < T_N/2,$$

where in general equality is achieved if and only if $\zeta_0 = 0$,

3) $R_{xx}(\tau)$ is strictly concave in the region $(-T_N/2, T_N/2)$,

4) The radius of curvature $r_c(\tau)$ of $R_{xx}(\tau)$ at $\tau = 0$ is inversely proportional to the signal's bandwidth, i.e.,

$$r_c(\tau)|_{\tau=0} = \frac{1}{R_{xx}(0)B_x}, \quad (\text{A-1})$$

where B_x is defined in (30) and is bounded from above by $\left(\frac{\pi}{T_N}\right)^2$,

5) The autocorrelation function $R_{xx}(\tau)$ is bounded in the region $\tau \in (-T_N/2, T_N/2)$, i.e.

$$\cos\left(\frac{\pi}{T_N}\tau\right) < \frac{R_{xx}(\tau)}{R_{xx}(0)} \leq 1 \quad \forall |\tau| < \frac{T_N}{2}. \quad (\text{A-2})$$

To prove the first property we use symmetry and real arguments of the power spectrum which results in

$$R_{xx}(\tau) = \frac{1}{2\pi} \int_{-\pi/T_N}^{\pi/T_N} S_{xx}(\Omega) \cos(\Omega\tau) d\Omega. \quad (\text{A-3})$$

We then note that in the interval of integration in eq. (A-3) $\cos(\Omega\tau) > 0$ for all $|\tau| < T_N/2$, which completes the proof since $S_{xx}(\Omega) \geq 0$ for all Ω . The second property follows by noting that

$$\begin{aligned} & \frac{1}{2} (R_{xx}(\tau - \zeta_0) + R_{xx}(\tau + \zeta_0)) = \\ & \frac{1}{2\pi} \int_{-\pi/T_N}^{\pi/T_N} S_{xx}(\Omega) \cos(\Omega\zeta_0) \cos(\Omega\tau) d\Omega, \end{aligned} \quad (\text{A-4})$$

and that for every $|\tau| < T_N/2$,

$$\frac{1}{2\pi} \int_{-\pi/T_N}^{\pi/T_N} S_{xx}(\Omega) \cos(\Omega\tau) \cdot (1 - \cos(\Omega\zeta_0)) d\Omega \geq 0. \quad (\text{A-5})$$

To show concavity of $R_{xx}(\tau)$, we differentiate eq. (A-3) twice with respect to τ , i.e.

$$R_{xx}''(\tau) = -\frac{1}{2\pi} \int_{-\pi/T_N}^{\pi/T_N} \Omega^2 S_{xx}(\Omega) \cos(\Omega\tau) d\Omega, \quad (\text{A-6})$$

and note that $R_{xx}''(\tau)$ is negative for all $|\tau| < T_N/2$, excluding the degenerate case where $S_{xx}(\Omega) = 2\pi R_{xx}(0)\delta(\Omega)$ in which $R_{xx}(\tau) = R_{xx}(0)$ and $R_{xx}''(\tau) = 0$. Noting that $R_{xx}'(\tau)|_{\tau=0} = 0$ and that

$$R_{xx}''(\tau)|_{\tau=0} = -\frac{1}{2\pi} \int_{-\pi/T_N}^{\pi/T_N} \Omega^2 S_{xx}(\Omega) d\Omega, \quad (\text{A-7})$$

it follows that the radius of curvature of $R_{xx}(\tau)$ at $\tau = 0$ is inversely proportional to B_x as defined in (30).

The lower bound in the fifth property follows by noting that in the region of integration in eq. (A-3),

$$\cos(\Omega\tau) \geq \cos\left(\frac{\pi}{T_N}\tau\right) \quad \forall |\tau| < \frac{T_N}{2}. \quad (\text{A-8})$$

Note that the lower bound cannot be achieved since $S_{xx}(\Omega)$ is assumed to be zero at $\Omega = \pm\frac{\pi}{T_N}$; however, we can get as close as we want to this lower bound. The upper bound is trivial.

APPENDIX B

RANDOMIZED SINC INTERPOLATION - MSE DERIVATION

The autocorrelation of $\hat{x}(t) = \sum_{n=-\infty}^{\infty} x[n]\tilde{h}(t - \tilde{t}_n)$ is

$$\begin{aligned} R_{\hat{x}\hat{x}}(t, t - \tau) &= E \left\{ \sum_{n=-\infty}^{\infty} x(nT + \xi_n) \tilde{h}(t - nT - \zeta_n) \cdot \right. \\ &\quad \left. \sum_{k=-\infty}^{\infty} x(kT + \xi_k) \tilde{h}(t - \tau - kT - \zeta_k) \right\}, \end{aligned} \quad (\text{B-1})$$

where $\tilde{h}(t) = \frac{T}{T_N} \cdot h(t)$. Using iterated expectation, we obtain

$$\begin{aligned} R_{\hat{x}\hat{x}}(t, t - \tau) &= \sum_{n=-\infty}^{\infty} \sum_{k=-\infty}^{\infty} E\{R_{xx}((n-k)T + \xi_n - \xi_k) \cdot \\ &\quad \tilde{h}(t - nT - \zeta_n) \cdot \tilde{h}(t - \tau - kT - \zeta_k)\} = \\ &= R_{xx}(0) \cdot \sum_{n=-\infty}^{\infty} E\{\tilde{h}(t - nT - \zeta_n) \tilde{h}(t - \tau - nT - \zeta_n)\} + \\ &\quad \sum_{n \neq k} E\{R_{xx}((n-k)T + \xi_n - \xi_k) \cdot \\ &\quad \tilde{h}(t - nT - \zeta_n) \cdot \tilde{h}(t - \tau - kT - \zeta_k)\}. \end{aligned} \quad (\text{B-2})$$

Representing $R_{xx}(t)$ and $\tilde{h}(t)$ in terms of their corresponding Fourier transforms $S_{xx}(\Omega)$ and $\tilde{H}(\Omega)$ and using the following identity:

$$\sum_n e^{j(\Omega_2 - \Omega_1)nT} = 2\pi \sum_k \delta((\Omega_2 - \Omega_1)T - 2\pi k), \quad (\text{B-3})$$

it follows that

$$\begin{aligned}
& \sum_{n=-\infty}^{\infty} E\{\tilde{h}(t - nT - \zeta_n)\tilde{h}(t - \tau - nT - \zeta_n)\} = \\
& E\left(\sum_{n=-\infty}^{\infty} \frac{1}{2\pi} \int_{-\Omega_c}^{\Omega_c} \tilde{H}(\Omega_1) e^{j\Omega_1(t-nT-\zeta_n)} d\Omega_1 \cdot \right. \\
& \left. \frac{1}{2\pi} \int_{-\Omega_c}^{\Omega_c} \tilde{H}^*(\Omega_2) e^{-j\Omega_2(t-\tau-nT-\zeta_n)} d\Omega_2\right) = \\
& \left(\frac{1}{2\pi}\right)^2 \int_{-\Omega_c}^{\Omega_c} \int_{-\Omega_c}^{\Omega_c} \tilde{H}(\Omega_1) \tilde{H}^*(\Omega_2) e^{j(\Omega_1-\Omega_2)t} e^{j\Omega_2\tau} \cdot \\
& \left(\sum_{n=-\infty}^{\infty} e^{j(\Omega_2-\Omega_1)nT}\right) \Phi_{\zeta}(\Omega_2 - \Omega_1) d\Omega_1 d\Omega_2 = \\
& \frac{1}{2\pi} \int_{-\Omega_c}^{\Omega_c} \frac{1}{T} |\tilde{H}(\Omega)|^2 e^{j\Omega\tau} d\Omega = \tilde{h}(\tau), \tag{B-4}
\end{aligned}$$

and

$$\begin{aligned}
& \sum_{n \neq k} E\{R_{xx}((n-k)T + \xi_n - \xi_k) \cdot \\
& \tilde{h}(t - nT - \zeta_n) \cdot \tilde{h}(t - \tau - kT - \zeta_k)\} = \\
& \sum_{n \neq k} E\left\{\frac{1}{2\pi} \int_{-\Omega_c}^{\Omega_c} S_{xx}(\Omega) e^{j\Omega((n-k)T + \xi_n - \xi_k)} d\Omega \cdot \right. \\
& \left. \frac{1}{2\pi} \int_{-\Omega_c}^{\Omega_c} \tilde{H}(\Omega_1) e^{j\Omega_1(t-nT-\zeta_n)} d\Omega_1 \cdot \right. \\
& \left. \frac{1}{2\pi} \int_{-\Omega_c}^{\Omega_c} \tilde{H}^*(\Omega_2) e^{-j\Omega_2(t-\tau-kT-\zeta_k)} d\Omega_2\right\} = \\
& \left(\frac{1}{2\pi}\right)^3 \int_{-\Omega_c}^{\Omega_c} \int_{-\Omega_c}^{\Omega_c} \int_{-\Omega_c}^{\Omega_c} S_{xx}(\Omega) \tilde{H}(\Omega_1) \tilde{H}^*(\Omega_2) \cdot \\
& \Phi_{\xi\zeta}(\Omega, -\Omega_1) \Phi_{\xi\zeta}^*(\Omega, -\Omega_2) \cdot e^{j(\Omega_1-\Omega_2)t} e^{j\Omega_2\tau} \cdot \\
& \sum_{n \neq k} \left(e^{j(\Omega-\Omega_1)nT} e^{-j(\Omega-\Omega_2)kT}\right) d\Omega d\Omega_1 d\Omega_2 = \\
& \left(\frac{1}{2\pi}\right)^3 \int_{-\Omega_c}^{\Omega_c} \int_{-\Omega_c}^{\Omega_c} \int_{-\Omega_c}^{\Omega_c} S_{xx}(\Omega) \tilde{H}(\Omega_1) \tilde{H}^*(\Omega_2) \cdot \\
& \Phi_{\xi\zeta}(\Omega, -\Omega_1) \Phi_{\xi\zeta}^*(\Omega, -\Omega_2) \cdot e^{j(\Omega_1-\Omega_2)t} e^{j\Omega_2\tau} \cdot \\
& \left(\sum_{n=-\infty}^{\infty} e^{j(\Omega-\Omega_1)nT} \sum_{k=-\infty}^{\infty} e^{-j(\Omega-\Omega_2)kT} - \right. \\
& \left. \sum_{n=-\infty}^{\infty} e^{j(\Omega_2-\Omega_1)nT}\right) d\Omega d\Omega_1 d\Omega_2 = \\
& \frac{1}{2\pi} \int_{-\Omega_c}^{\Omega_c} \frac{1}{T} |\tilde{H}(\Omega)|^2 \left[\frac{1}{T} S_{xx}(\Omega) \cdot |\Phi_{\xi\zeta}(\Omega, -\Omega)|^2 - \right. \\
& \left. \frac{1}{2\pi} \int_{-\Omega_c}^{\Omega_c} S_{xx}(\Omega_1) |\Phi_{\xi\zeta}(\Omega_1, -\Omega)|^2 d\Omega_1\right] e^{j\Omega\tau} d\Omega. \tag{B-5}
\end{aligned}$$

Substituting (B-5) and (B-4) in (B-2) results in

$$\begin{aligned}
R_{\hat{x}\hat{x}}(t, t - \tau) &= \frac{1}{2\pi} \int_{-\Omega_c}^{\Omega_c} S_{xx}(\Omega) \cdot |\Phi_{\xi\zeta}(\Omega, -\Omega)|^2 e^{j\Omega\tau} d\Omega + \tag{B-6} \\
&\frac{T}{2\pi} \int_{-\Omega_c}^{\Omega_c} \left(\frac{1}{2\pi} \int_{-\Omega_c}^{\Omega_c} S_{xx}(\Omega_1) \cdot (1 - |\Phi_{\xi\zeta}(\Omega_1, -\Omega)|^2) d\Omega_1\right) e^{j\Omega\tau} d\Omega.
\end{aligned}$$

Similarly, the cross correlation of $\hat{x}(t)$ and $x(t)$ can be expressed as

$$\begin{aligned}
R_{\hat{x}x}(t, t - \tau) &= E(\hat{x}(t)x(t - \tau)) = \\
& E\left\{\sum_{n=-\infty}^{\infty} x(nT + \xi_n) \tilde{h}(t - nT - \zeta_n) \cdot x(t - \tau)\right\} = \\
& E\left\{\sum_{n=-\infty}^{\infty} R_{xx}(\tau + nT + \xi_n - t) \tilde{h}(t - nT - \zeta_n)\right\} = \\
& \left(\frac{1}{2\pi}\right)^2 \int_{-\Omega_c}^{\Omega_c} \int_{-\Omega_c}^{\Omega_c} S_{xx}(\Omega) \tilde{H}(\Omega_1) \Phi_{\xi\zeta}(\Omega, -\Omega_1) \cdot \\
& e^{j(\Omega_1-\Omega)t} e^{j\Omega\tau} \left(\sum_{n=-\infty}^{\infty} e^{j(\Omega-\Omega_1)nT}\right) d\Omega_1 d\Omega = \\
& \frac{1}{2\pi} \int_{-\Omega_c}^{\Omega_c} S_{xx}(\Omega) \cdot \Phi_{\xi\zeta}(\Omega, -\Omega) e^{j\Omega\tau} d\Omega, \tag{B-7}
\end{aligned}$$

where in the last transition we used again the identity in (B-3).

Taking the Fourier transform of (B-7) and (B-7) with respect to τ results in

$$\begin{aligned}
S_{\hat{x}\hat{x}}(\Omega) &= \frac{T}{2\pi} \int_{-\Omega_c}^{\Omega_c} S_{xx}(\Omega_1) \cdot (1 - |\Phi_{\xi\zeta}(\Omega_1, -\Omega)|^2) d\Omega_1 + \\
& S_{xx}(\Omega) \cdot |\Phi_{\xi\zeta}(\Omega, -\Omega)|^2 \quad |\Omega| < \Omega_c \tag{B-8}
\end{aligned}$$

and

$$S_{\hat{x}x}(\Omega) = S_{xx}(\Omega) \cdot \Phi_{\xi\zeta}(\Omega, -\Omega) \quad |\Omega| < \Omega_c, \tag{B-9}$$

from which the second-order statistics model of Figure 2 clearly follows.

The power spectrum of the reconstruction error $e^R(t) = \hat{x}(t) - x(t)$ is

$$S_{e^R e^R}(\Omega) = S_{\hat{x}\hat{x}}(\Omega) - S_{\hat{x}x}(\Omega) - S_{x\hat{x}}(\Omega) + S_{xx}(\Omega), \tag{B-10}$$

where $S_{\hat{x}\hat{x}}(\Omega)$ and $S_{\hat{x}x}(\Omega)$ are given in (B-8) and (B-9) respectively, and $S_{x\hat{x}}(\Omega) = S_{\hat{x}x}^*(\Omega)$. Consequently,

$$\begin{aligned}
S_{e^R e^R}(\Omega) &= S_{xx}(\Omega) \cdot |1 - \Phi_{\xi\zeta}(\Omega, -\Omega)|^2 + \\
& \frac{T}{2\pi} \int_{-\Omega_c}^{\Omega_c} S_{xx}(\Omega_1) \cdot [1 - |\Phi_{\xi\zeta}(\Omega_1, -\Omega)|^2] d\Omega_1 \quad |\Omega| < \Omega_c.
\end{aligned}$$

Integrating the power spectrum over frequency, we obtain the MSE, i.e.,

$$E(\{e^R(t)\}^2) = \frac{1}{2\pi} \int_{-\Omega_c}^{\Omega_c} S_{e^R e^R}(\Omega) d\Omega = \tag{B-11}$$

$$\begin{aligned}
& \frac{1}{2\pi} \int_{-\Omega_c}^{\Omega_c} S_{xx}(\Omega) \cdot |1 - \Phi_{\xi\zeta}(\Omega, -\Omega)|^2 d\Omega + \\
& \frac{T}{T_N} \cdot \frac{1}{2\pi} \int_{-\Omega_c}^{\Omega_c} S_{xx}(\Omega) d\Omega - \\
& \frac{T}{T_N} \cdot \frac{1}{2\pi} \int_{-\Omega_c}^{\Omega_c} S_{xx}(\Omega) \cdot \left(\frac{1}{2\Omega_c} \int_{-\Omega_c}^{\Omega_c} |\Phi_{\xi\zeta}(\Omega, -\Omega_1)|^2 d\Omega_1\right) d\Omega.
\end{aligned}$$

APPENDIX C
SUB-NYQUIST SAMPLING - RSI

The autocorrelation of $\hat{x}(t) = \sum_{n=-\infty}^{\infty} x(t_n)h_T(t - \tilde{t}_n)$ is

$$\begin{aligned} R_{\hat{x}\hat{x}}(t, t - \tau) &= E \left(\sum_{n=-\infty}^{\infty} x(nT + \xi_n) h_T(t - nT - \zeta_n) \cdot \right. \\ &\quad \left. \sum_{k=-\infty}^{\infty} x(kT + \xi_k) h_T(t - \tau - kT - \zeta_k) \right) = \\ &= R_{xx}(0) \cdot E \left(\sum_{n=-\infty}^{\infty} h_T(t - nT - \zeta_n) h_T(t - \tau - nT - \zeta_n) \right) + \\ &\quad \sum_{n \neq k} E(R_{xx}((n - k)T + \xi_n - \xi_k) \cdot \\ &\quad h_T(t - nT - \zeta_n) h_T(t - \tau - kT - \zeta_k)), \end{aligned} \quad (C-1)$$

where $h_T(t) = \text{sinc}(\frac{\pi}{T}t)$. Representing $R_{xx}(t)$ and $h_T(t)$ in terms of $S_{xx}(\Omega)$ and $H_T(\Omega)$, we obtain

$$\begin{aligned} &\sum_{n \neq k} E(R_{xx}((n - k)T + \xi_n - \xi_k) h_T(t - nT - \zeta_n) \cdot \\ &\quad h_T(t - \tau - kT - \zeta_k)) = \left(\frac{1}{2\pi} \right)^3 \int_{-\Omega_c}^{\Omega_c} \int_{-\frac{\pi}{T}}^{\frac{\pi}{T}} \int_{-\frac{\pi}{T}}^{\frac{\pi}{T}} S_{xx}(\Omega) \cdot \\ &\quad H_T(\Omega_1) H_T^*(\Omega_2) e^{j(\Omega_1 - \Omega_2)t} e^{j\Omega_2\tau} \cdot \Phi_{\xi\zeta}(\Omega, -\Omega_1) \Phi_{\xi\zeta}^*(\Omega, -\Omega_2) \cdot \\ &\quad \left(\sum_{n \neq k} e^{j(\Omega - \Omega_1)nT} e^{-j(\Omega - \Omega_2)kT} \right) d\Omega d\Omega_1 d\Omega_2 = \\ &\quad \frac{1}{2\pi} \int_{-\frac{\pi}{T}}^{\frac{\pi}{T}} \left(\sum_{n=-\infty}^{\infty} S_{xx} \left(\Omega - \frac{2\pi}{T}n \right) \cdot \left| \Phi_{\xi\zeta} \left(\Omega - \frac{2\pi}{T}n, -\Omega \right) \right|^2 - \right. \\ &\quad \left. \frac{T}{2\pi} \int_{-\Omega_c}^{\Omega_c} S_{xx}(\Omega_1) |\Phi_{\xi\zeta}(\Omega_1, -\Omega)|^2 d\Omega_1 \right) e^{j\Omega_2\tau} d\Omega, \end{aligned} \quad (C-2)$$

and

$$\begin{aligned} &E \left(\sum_{n=-\infty}^{\infty} h_T(t - nT - \zeta_n) h_T(t - \tau - nT - \zeta_n) \right) = \\ &= E \left(\sum_{n=-\infty}^{\infty} \frac{1}{2\pi} \int_{-\frac{\pi}{T}}^{\frac{\pi}{T}} H_T(\Omega_1) e^{j\Omega_1(t - nT - \zeta_n)} d\Omega_1 \cdot \right. \\ &\quad \left. \frac{1}{2\pi} \int_{-\frac{\pi}{T}}^{\frac{\pi}{T}} H_T^*(\Omega_2) e^{-j\Omega_2(t - \tau - nT - \zeta_n)} d\Omega_2 \right) = \\ &\quad \left(\frac{1}{2\pi} \right)^2 \int_{-\frac{\pi}{T}}^{\frac{\pi}{T}} \int_{-\frac{\pi}{T}}^{\frac{\pi}{T}} H_T(\Omega_1) H_T^*(\Omega_2) e^{j(\Omega_1 - \Omega_2)t} e^{j\Omega_2\tau} \cdot \\ &\quad \left(\sum_{n=-\infty}^{\infty} e^{j(\Omega_2 - \Omega_1)nT} \right) \Phi_{\xi\zeta}(\Omega_2 - \Omega_1) d\Omega_1 d\Omega_2 = h_T(\tau). \end{aligned} \quad (C-3)$$

Substituting (C-2) and (C-3) into (C-1) and taking the Fourier transform with respect to τ , we obtain

$$\begin{aligned} S_{\hat{x}\hat{x}}(\Omega) &= \sum_{n=-\infty}^{\infty} S_{xx} \left(\Omega - \frac{2\pi}{T}n \right) \left| \Phi_{\xi\zeta} \left(\Omega - \frac{2\pi}{T}n, -\Omega \right) \right|^2 + \\ &\quad \frac{T}{2\pi} \int_{-\Omega_c}^{\Omega_c} S_{xx}(\Omega_1) (1 - |\Phi_{\xi\zeta}(\Omega_1, -\Omega)|^2) d\Omega_1 \quad |\Omega| < \frac{\pi}{T}. \end{aligned} \quad (C-4)$$

The cross-correlation of $\hat{x}(t)$ and $x(t)$ is

$$\begin{aligned} R_{\hat{x}x}(t, t - \tau) &= E \left(\sum_{n=-\infty}^{\infty} x(nT + \xi_n) h_T(t - nT - \zeta_n) x(t - \tau) \right) \\ &= \sum_{n=-\infty}^{\infty} E(R_{xx}(nT + \xi_n + \tau - t) h_T(t - nT - \zeta_n)), \end{aligned} \quad (C-5)$$

where, again, by representing $R_{xx}(t)$ and $h_T(t)$ in terms of $S_{xx}(\Omega)$ and $H_T(\Omega)$, we obtain

$$\begin{aligned} R_{\hat{x}x}(t, t - \tau) &= \frac{1}{2\pi} \int_{-\frac{\pi}{T}}^{\frac{\pi}{T}} \sum_{n=-\infty}^{\infty} \left(S_{xx} \left(\Omega - \frac{2\pi}{T}n \right) \cdot \right. \\ &\quad \left. \Phi_{\xi\zeta} \left(\Omega - \frac{2\pi}{T}n, -\Omega \right) e^{j\frac{2\pi}{T}n(t - \tau)} \right) e^{j\Omega\tau} d\Omega. \end{aligned} \quad (C-6)$$

An alternative representation is obtained by representing $S_{xx}(\Omega)$ and $\Phi_{\xi\zeta}(\Omega_1, \Omega_2)$ in terms of $R_{xx}(t)$ and $f_{\xi\zeta}(\xi, \zeta)$, i.e.,

$$\begin{aligned} R_{\hat{x}x}(t, t - \tau) &= \int_{-\infty}^{\infty} R_{xx}(t_1) \cdot \\ &\quad \sum_{n=-\infty}^{\infty} \left[f_{\xi\zeta}(t_1 + t - nT - \tau, \zeta) * h_T \left(\frac{\pi}{T}\zeta \right) \right] |_{\zeta=t-nT} dt_1 \end{aligned} \quad (C-7)$$

REFERENCES

- [1] R. Amirtharajah, J. Collier, J. Siebert, B. Zhou, and A. Chandrakasan, "Dsps for energy harvesting sensors: applications and architectures," *IEEE Pervasive Computing*, vol. 4, no. 3, pp. 72–79, July 2005.
- [2] J. L. Yen, "On nonuniform sampling of bandwidth-limited signals," *IRE Trans. Circuit Theory*, vol. 3, no. 4, pp. 251–257, 1956.
- [3] D. P. Mitchell, "Generating antialiased images at low sampling densities," *International Conference on Computer Graphics and Interactive Techniques*, vol. 5, no. 1, pp. 65–72, January 1987.
- [4] A. Papoulis, "Generalized sampling expansion," *IEEE Trans. Circuits and Systems*, vol. CAS-24, no. 11, pp. 652–654, 1977.
- [5] A. J. Jerri, "The shannon sampling theorem-its various extensions and applications: A tutorial review," *Proceedings of the IEEE*, vol. 65, no. 11, pp. 1565–1596, 1977.
- [6] Y. C. Eldar and A. V. Oppenheim, "Filterbank reconstruction of bandlimited signals from nonuniform and generalized samples," *IEEE Trans. Signal Processing*, vol. 48, no. 10, pp. 2864–2875, 2000.
- [7] T. Strohmer and J. Tanner, "Fast reconstruction methods for bandlimited functions from periodic nonuniform sampling," *SIAM J. Numer. Anal.*, vol. 44, no. 3, pp. 1073–1094, 2006.
- [8] S. Maymon and A. V. Oppenheim, "Quantization and compensation in sampled interleaved multi-channel systems," *ICASSP 2010, IEEE International Conference on Acoustics, Speech and Signal Processing*, March 2010.
- [9] K. Yao and J. B. Thomas, "On some stability and interpolatory properties of nonuniform sampling expansions," *IEEE Trans. Circuit Theory*, vol. CT-14, no. 4, pp. 404–408, 1967.

- [10] N. Levinson, *Gap and Density Theorems*. American Mathematical Society, 1940.
- [11] C. D. Boor, "On calculating with b-splines," *J. Approximat. Theory*, vol. 6, pp. 50–62, 1970.
- [12] R. G. Wiley, "Recovery of band-limited signals from unequally spaced samples," *IEEE Trans. Comm.*, vol. COM-26, no. 1, Jan. 1978.
- [13] F. Marvasti, "Spectral analysis of random sampling and error free recovery by an iterative method," *IECE Trans. Inst. Electron. Commun. Eng., Japan (Sect. E)*, vol. E-69, no. 2, Feb. 1986.
- [14] F. Marvasti and M. Analoui, "Recovery of signals from nonuniform samples using iterative methods," *IEEE Proceedings of International Conference on Circuits and Systems, Oregon*, July 1989.
- [15] F. Marvasti, M. Analoui, and M. Gamshadzahi, "Recovery of signals from nonuniform samples using iterative methods," *IEEE Trans. Acoust., Speech, Signal Processing*, April 1991.
- [16] H. G. Feichtinger and K. Grochenig, "Irregular sampling theorems and series expansions of band-limited functions," *J. Math. Anal. and Appl.*, vol. 167, pp. 530–556, 1992.
- [17] K. Grochenig, "Reconstruction algorithms in irregular sampling," *Math. Comp.*, vol. 59, no. 199, pp. 181–194, July 1992.
- [18] H. G. Feichtinger, K. Grochenig, and T. Strohmer, "Efficient numerical methods in non-uniform sampling theory," *Numerische Mathematik*, vol. 69, no. 4, pp. 423–440, July 1995.
- [19] A. Papoulis, "Error analysis in sampling theory," *Proceedings of the IEEE*, vol. 54, no. 7, pp. 947–955, July 1966.
- [20] J. J. Clark, M. R. Palmer, and P. D. Lawrence, "A transformation method for the reconstruction of functions from nonuniformly spaced samples," *IEEE Trans. Acoust., Speech, Signal Processing*, vol. ASSP-33, no. 4, pp. 1151–1165, October 1985.
- [21] Y. Y. Zeevi and E. Shlomot, "Nonuniform sampling and antialiasing in image representation," *IEEE Trans. Signal Processing*, vol. 41, no. 3, pp. 1223–1236, March 1993.
- [22] A. Tarczynski, "FIR filters for systems with input clock jitter," *Circuits and Systems, 2001. Iscas2001*, vol. 2, pp. 617–620, 2001.
- [23] A. V. Balakrishnan, "On the problem of time jitter in sampling," *IRE Trans. Inform. Theory*, vol. 8, pp. 226–236, 1962.
- [24] S. Maymon and A. Oppenheim, "Randomized sinc interpolation of nonuniform samples," *EUSIPCO 2009, 17th European Signal Processing Conference*, August 2009.
- [25] O. A. Z. Leneman and J. B. Lewis, "Random sampling of random processes: Mean-square comparison of various interpolators," *IEEE Transactions on Automatic Control*, vol. 11, no. 3, pp. 396–403, July 1966.
- [26] J. Selva, "Functionally weighted lagrange interpolation of band-limited signals from nonuniform samples," *Trans. Sig. Proc.*, vol. 57, no. 1, January 2009.
- [27] J. R. Higgins, *Sampling Theory in Fourier and Signal Analysis: Foundations*. Oxford: Oxford Science Publications, Clarendon Press, 1996.
- [28] F. Marvasti, *Nonuniform Sampling*. New York: Kluwer Academic, 2001.
- [29] M. Unser, "Sampling - 50 years after shannon," *Proceedings of the IEEE*, vol. 88, no. 4, pp. 569–587, April 2000.
- [30] H. S. Shapiro and R. A. Silverman, "Alias-free sampling of random noise," *Journal of the Society for Industrial and Applied Mathematics*, vol. 8, no. 2, pp. 225–248, 1960.
- [31] R. L. Cook, "Stochastic sampling in computer graphics," *ACM Transactions on Graphics*, vol. 5, no. 1, pp. 51–72, January 1986.
- [32] P. D. Welch, "The use of fast fourier transform for the estimation of power spectra: A method based on time averaging over short, modified periodograms," *IEEE Transactions on Audio Electroacoustics*, vol. AU-15, p. 7073, 1967.



Shay Maymon graduated from Tel-Aviv University (TAU), Tel-Aviv, Israel, in June 1998 with a B.Sc. in Electrical Engineering. In June 1999 he was awarded his M.Sc. from TAU. Following six years' military service as an R&D engineer and an intelligence officer in a leading technological unit of the Israel Defense Forces (IDF), he is currently pursuing his Ph.D. in the Digital Signal Processing Group at MIT. His research interests within the area of Signal Processing include Sampling, Detection and Estimation Theory.

From 2007 to 2009 he held the Fulbright fellowship for Ph.D studies in Electrical Engineering at MIT. He has received a number of awards including the Yitzhak and Chaya Weinstein Study Prize and the President and Rector Award for outstanding graduate students at TAU. Promoted to Instructor-G at MIT in 2008, he has received a number of awards for teaching, including the Frederick C. Hennie Teaching Award for Teaching Excellence at MIT for the years 2007-2009 and the Dean's Award for Teaching Excellence at TAU for the years 2001/2002, 2004/05-2006/07.



Alan V. Oppenheim was born in New York, New York on November 11, 1937. He received S.B. and S.M. degrees in 1961 and an Sc.D. degree in 1964, all in Electrical Engineering, from the Massachusetts Institute of Technology. He is also the recipient of an honorary doctorate from Tel Aviv University.

In 1964, Dr. Oppenheim joined the faculty at MIT, where he is currently Ford Professor of Engineering. Since 1967 he has been affiliated with MIT Lincoln Laboratory and since 1977 with the Woods Hole Oceanographic Institution. His research interests are in the general area of signal processing and its applications. He is coauthor of the widely used textbooks *Discrete-Time Signal Processing* and *Signals and Systems*. He is also editor of several advanced books on signal processing.

Dr. Oppenheim is a member of the National Academy of Engineering, a fellow of the IEEE, and a member of Sigma Xi and Eta Kappa Nu. He has been a Guggenheim Fellow and a Sackler Fellow. He has received a number of awards for outstanding research and teaching, including the IEEE Education Medal, the IEEE Jack S. Kilby Signal Processing Medal, the IEEE Centennial Award and the IEEE Third Millennium Medal. From the IEEE Signal Processing Society he has been honored with the Education Award, the Society Award, the Technical Achievement Award and the Senior Award. He has also received a number of awards at MIT for excellence in teaching, including the Bose Award and the Everett Moore Baker Award.